






Vision-Centric Representation-Efficient Fine-Tuning for Robust Universal Foreground Segmentation

Guoyi Zhang , Siyang Chen , Guangsheng Xu , Han Wang , and Xiaohu Zhang 

Abstract—Foreground segmentation is crucial for scene understanding, yet parameter-efficient fine-tuning (PEFT) of vision foundation models (VFM) often fails in complex scenarios, such as camouflage and infrared imagery. We attribute this challenge to the inherent texture bias in VFMs, which is exacerbated during fine-tuning and limits generalization in texture-sparse environments. To address this, we propose Ladder Shape-bias Representation Side-tuning (LSR-ST), a lightweight PEFT framework that enhances model robustness by introducing shape-biased inductive priors. LSR-ST captures shape-aware features using a simple HDConv Block, which integrates large-kernel attention and residual learning. The method satisfies three key conditions for inducing shape bias: large receptive fields, multi-order feature interactions, and sparse connectivity. Our analysis reveals that these improvements stem from “*representation efficiency*”—the ability to extract task-relevant, structurally grounded features while minimizing redundancy. We formalize this concept via Information Bottleneck theory and advocate for it as a key PEFT objective. Unlike traditional NLP paradigms that focus on optimizing parameters and memory, visual tasks require models that extract *task-defined* semantics, rather than just relying on *pre-encoded* features. This shift enables our approach to move beyond conventional trade-offs, offering more robust and generalizable solutions for vision tasks. With minimal changes to SAM2-UNet, LSR-ST achieves consistent improvements across 17 datasets and 6 tasks using only 4.719M trainable parameters. These results highlight the potential of representation efficiency for robust and adaptable VFMs within complex visual environments.

Index Terms—Foreground segmentation, vision foundation model, representation learning, representation-efficient fine-tuning.

I. INTRODUCTION

FOREGROUND segmentation is a core problem in scene understanding, which seeks to distinguish the foreground from the background by utilizing contextual information [1]. This task is pivotal in a wide range of computer vision applications, such as camouflaged object detection [2], salient object detection [3], mirror detection [4], marine animal segmentation [5], shadow detection [6], and infrared small target detection [7]. Traditional approaches typically design specialized algorithms for each subtask, often relying on domain-specific knowledge and handcrafted priors, including edge [8] or frequency-domain features [4]. However, such methods often suffer from

limited generalizability and robustness across diverse real-world scenarios [9].

Recent advancements in vision foundation models [10]–[13], particularly those built upon the Vision Transformer (ViT) architecture, have significantly propelled progress in the field [14]–[16]. Trained on large-scale datasets, these models have demonstrated remarkable generalization capabilities and achieved SOTA performance across a wide spectrum of visual tasks. With the adoption of parameter-efficient fine-tuning techniques [17], high-performance and task-agnostic foreground segmentation has become increasingly feasible. In particular, a recent line of work [18]–[20] has investigated the use of vision foundation models, particularly the Segment Anything Model (SAM) family [10], [11], for universal foreground segmentation [21], achieving SOTA performance across a range of sub-tasks.

However, existing methods struggle to generalize to complex downstream scenarios, particularly when faced with weakly textured infrared images [14] or camouflaged scenes, where the foreground and background share similar textures [22], leading to significant performance degradation. To alleviate these challenges, a number of studies have attempted to incorporate task-specific priors, including frequency-domain signals and edge features, into parameter-efficient fine-tuning frameworks [1], [14], [19], [20], [23]. While these approaches have achieved promising results in certain narrowly defined tasks [24], their generalization remains limited. Nevertheless, these approaches often suffer from high computational complexity, sensitivity to hyperparameter settings, and substantial memory overhead [25]. Moreover, such priors typically lack universality, further constraining the generalization ability and robustness of the resulting models [24]. **More critically**, these methods lack a rigorous analysis of the underlying challenges and fail to develop a deep understanding of the root causes behind performance degradation. As a result, many of these efforts lead to overly complex, brittle solutions and unsustainable progress.

To address the aforementioned challenges, the first key question this study seeks to answer is: ***What causes vision foundation models with parameter-efficient fine-tuning to underperform in complex downstream scenarios?***

This question, in fact, can be effectively addressed through a deeper understanding of the **representational biases inherent** in vision foundation models. Specifically, vision foundation models exhibit a pronounced texture bias [26]–[29], making them highly sensitive to texture-related cues and largely reliant on texture features for image analysis. While this bias contributes to their strong performance in tasks involving salient object detection [30]—where texture and color play

Manuscript received xxx, xxx; revised xxx, xxx.

Equal contribution: Guoyi Zhang and Siyang Chen.

Corresponding authors: Xiaohu Zhang.

Guoyi Zhang, Siyang Chen, Guangsheng Xu, Han Wang, and Xiaohu Zhang are with the School of Aeronautics and Astronautics, Sun Yat-sen University, Shenzhen 518107, Guangdong, China.(email: {zhanggy57, chensy253, xugsh6, wangh737}@mail2.sysu.edu.cn; zhangxiaohu@mail.sysu.edu.cn)

dominant roles—it significantly hinders their effectiveness in scenarios such as infrared imagery and camouflage, where texture information is weak or misleading [18]. Even more critically, **fine-tuning** these models can further **amplify** the underlying texture bias, leading them to overfit to superficial texture patterns [31], [32]. As a result, their performance deteriorates in complex downstream tasks that require strong semantic or structural understanding [22], [33].

Given that texture bias limits the effectiveness of parameter-efficient fine-tuning in complex scenarios, the second key question this study addresses is: *How can we alleviate texture bias while preserving texture sensitivity for tasks that depend on it?*

The answer lies in **introducing shape-biased representations**—that is, enhancing the model’s ability to attend to structural, contextual, and shape-related cues during feature extraction [34]. This capability forms the foundation for robust object understanding and accurate recognition in challenging environments. Prior studies [35]–[37] have shown that incorporating shape bias into texture-biased neural networks leads to more robust and generalizable representations, enabling better adaptation to complex tasks without compromising performance on texture-centric ones. Notably, the human visual system effectively integrates both shape and texture information in the spatial domain [38], demonstrating strong generalization and resilience under diverse real-world conditions.

A particularly important distinction worth highlighting is the difference between **shape-biased representations** and **frequency-domain methods**. While it is well known that high-frequency components in the frequency domain implicitly encode shape information [39], this implicit encoding is fundamentally different from explicit shape representations. Specifically: (1) frequency-domain features often entangle foreground and background signals, making them prone to overfitting to specific datasets [25]; (2) the frequency bands corresponding to target-relevant information vary across images, and the coupling of background noise further complicates the effective use of handcrafted or learned frequency-domain priors, making adaptive frequency selection highly challenging; and (3) implicit cues are generally less effective than explicit structural representations in downstream tasks [40].

It is important to emphasize that **this distinction does not discredit frequency-based approaches**. On the contrary, frequency-domain fine-tuning techniques have made significant contributions to a wide range of vision tasks, such as object detection and depth estimation [39]. Rather, our intention is to offer a new perspective for understanding and addressing the limitations of parameter-efficient fine-tuning in vision foundation models—particularly in the SAM family [10], [11]—when applied to complex downstream scenarios. We further believe that, in the future, cross-validation between spatial (shape-aware) and frequency-domain representations may foster deeper synergy and lead to more robust and generalizable visual systems.

Naturally, the third key question this study aims to answer is: *How can shape bias be effectively introduced into parameter-efficient fine-tuning?*

To address this question, we first identify the architec-

tural conditions under which shape-biased representations can emerge. Unlike previous works that attribute representational bottlenecks solely to large effective receptive fields [41]–[44], we identify three key factors: **(1) large effective receptive field** [34], [45]–[48]. Models with larger receptive fields tend to exhibit stronger shape bias [49], and architectures utilizing large-kernel convolutions have demonstrated superior shape-bias capabilities compared to ViTs [34]. For these models, shape bias representation improves as the size of the convolution kernel increases [45], [46], [50]. Additionally, it is crucial for the receptive field size to be dynamically allocated to adapt to varying spatial patterns [51]; **(2) multi-order feature interactions** [52], [53]. In contrast to self-attention or convolution, which primarily focus on global or local features, intermediate-level feature interactions—mirroring those in human perception—are essential for robust object recognition [54]. Moreover, empirical studies in few-shot learning suggest that mid-level features generalize more effectively [55]. Additionally, insights from *multi-agent game theory* [56]–[59] indicate that overly complex or overly simplistic interactions can result in non-robust representations; and **(3) sparse connections** [50], [60], [61]. Sparse connections, inspired by sparse coding in the human brain [62], facilitate structural encoding in neural networks [60], enabling the decomposition of objects into parts and subparts—thereby fostering shape-bias representations [63].

Building upon this foundation, we propose a simple yet highly effective parameter-efficient fine-tuning method. Many studies suggest [64] that the added complexity in the design of current deep learning models often obscures the true underlying factors that contribute to their effectiveness. The core principle of our approach is to minimize design noise, clearly presenting our central idea while validating its effectiveness. In line with this principle, our method leverages well-established deep learning design practices. Specifically, we introduce **Ladder Shape-bias Representation Side-tuning (LSR-ST)**, which builds upon the ladder side-tuning framework [65]. The side network captures image features independently, and its loose coupling with the backbone significantly reduces memory usage during training [66]. To equip the side network with both shape-biased representations and task-specific feature learning, we design a lightweight convolutional module, called the **HDConv Block**. This block incorporates a shape-enhanced large-kernel attention mechanism as the token mixer to capture structural information, and a pre-activation residual module [67] as the channel mixer to learn task-relevant features.

To validate the effectiveness of our method, we adopt SAM2-UNet [18]—a strong and general-purpose foreground segmentation baseline. We retain all of its original hyperparameter settings, with only the fine-tuning strategy being replaced by ours. With only 4.719M learnable parameters, our method achieves significant improvements across **17 public datasets** spanning **six downstream tasks**, including camouflaged object detection, salient object detection, mirror detection, shadow detection, infrared small target detection, and marine animal segmentation. Our method demonstrates substantial improvements, particularly in challenging scenarios with weak texture or camouflaged targets, while still showing gains in tasks that depend on texture analysis, thus confirming

the robustness introduced by shape-biased representations. Extensive comparisons with **multiple SOTA methods across various sub-tasks** further validate the effectiveness of our approach.

Building on the recognition that existing PEFT methods struggle with generalization in complex visual tasks, we propose a novel approach to address these limitations. Unlike NLP paradigms that optimize parameters and memory, visual tasks require models to extract **task-defined** semantics, not just **intrinsically encoded** features. Our investigation shows that merely adhering to NLP-inspired paradigms is insufficient for robust performance. By aligning the model’s representation preferences with the task’s specific needs within PEFT, we achieve substantial improvements in complex tasks. This leads us to introduce **“representation efficiency”**, which balances extracting task-relevant features with minimizing redundancy, offering a more comprehensive approach than traditional efficiency metrics. Grounded in **Information Bottleneck (IB) theory** [68], we define representation efficiency as maximizing mutual information with the task while minimizing dependence on raw input. This shift enables our approach to move beyond conventional trade-offs, providing a more robust and generalizable foundation for improving vision foundation models.

We summarize the main contributions as follows:

- We conduct a systematic analysis revealing that the inherent **texture bias** in vision foundation models is a key factor limiting their robustness and adaptability in visually complex scenarios.
- We propose **LSR-ST**, a simple yet effective fine-tuning framework that incorporates shape-biased representations by design, significantly improving generalization in challenging vision tasks.
- We identify and consolidate three architectural principles essential for inducing shape bias: **large effective receptive fields**, **multi-order feature interactions**, and **sparse connectivity**.
- We develop the **HDCConv Block**, a lightweight module featuring shape-enhanced large-kernel attention, to facilitate efficient and robust structure-aware learning within the side network.
- With only minimal modifications to the SAM2-UNet baseline [18], our approach achieves consistent improvements across **17 datasets and 6 downstream tasks**, without sacrificing performance on texture-sensitive benchmarks.
- We introduce the notion of **“representation efficiency”**, inspired by **Information Bottleneck theory** [68], as a complementary objective to traditional PEFT metrics. It encourages the learning of task-relevant, structure-aware representations while minimizing redundancy.

The remainder of this paper is organized as follows: Section II briefly reviews related work. Section III discusses the motivation for introducing the concept of **“representation efficiency”**. Section IV presents the proposed method in detail. Experimental results and analysis are provided in Section V. Finally, Section VI concludes the paper.

II. RELATED WORK

We briefly review related works from four aspects: universal foreground segmentation, parameter-efficient fine-tuning, shape-bias representation learning, and large-kernel networks.

A. Universal Foreground Segmentation

Foreground segmentation is a fundamental task in scene understanding, supporting various downstream applications. Traditional approaches often design task-specific algorithms for each sub-task, relying on handcrafted priors [69]–[71], which limits generalizability. With the rise of vision foundation models (VFM), recent works have explored parameter-efficient fine-tuning for universal foreground segmentation. For instance, EVP and FGSA Net [1], [19], [23] incorporated frequency-domain cues to address challenges like camouflaged object detection, but face issues like high complexity and limited generalization. FOCUS [20] fine-tuned DINOv2 [12] using CLIP [72] to improve segmentation, but with a large overhead of 1.2G parameters. Recently, SAM2-UNet [18] proposed a U-shaped encoder-decoder with multi-scale fine-tuning for SAM2, achieving competitive results across various sub-tasks but struggling in complex downstream scenarios.

Unlike previous works, we analyze the texture bias inherent in foundation models from a representation learning perspective, which leads to suboptimal performance in complex downstream tasks. We focus on introducing shape-biased representations through parameter-efficient fine-tuning, which improves performance in both structure-critical and texture-reliant tasks.

B. Parameter-efficient Fine-tuning

Parameter-efficient fine-tuning (PEFT) [1], [17], [19], [23] enables vision foundation models to adapt to downstream tasks using only a small number of trainable parameters by concentrating on task-specific knowledge. However, most existing approaches are heavily inspired by paradigms developed for natural language processing (NLP), and thus primarily emphasize improvements in parameter [73], memory [65], [74], [75], and training efficiency [76]. While effective in NLP, this paradigm may not be well suited to the unique characteristics of visual tasks, often resulting in suboptimal performance in complex scenarios.

Unlike previous works, we propose considering representation efficiency in addition to parameter, memory, and training efficiency. Specifically, to address the performance degradation of the SAM family in complex downstream tasks, we focus on introducing shape bias through parameter-efficient fine-tuning to improve robustness in such scenarios. Our approach builds on the Ladder side-tuning framework [65], where the side network independently captures task-specific representations, allowing for more effective adaptation to diverse tasks.

C. Shape-bias Representation Learning

Representation learning has been a key driver in the development of vision models [77]–[79]. Many studies [27], [35]–[38], [60], [80], [81] have attempted to introduce shape-biased representations to mitigate the inherent texture bias

in models, aligning them with human visual perception and enhancing robustness in downstream tasks. However, most of the existing works focus on classification tasks and introduce shape regularization terms through novel data augmentations or loss functions [38]. On the model design side, prior work often combines edge priors [8], [82], but such priors only hold in specific cases, limiting the adaptability of the models. Other studies have focused on expanding the effective receptive field size [34], [46]–[48], [50], [61], but this often leads to representational bottlenecks.

In contrast to the aforementioned works, we attempt to introduce shape bias into vision foundation models through parameter-efficient fine-tuning to enhance effectiveness in complex scenarios. Furthermore, we identify three key conditions in model design—large effective receptive fields, multi-order feature interactions, and sparse connections—that can effectively overcome representational bottlenecks, particularly when the number of tunable parameters is small, demonstrating high performance.

D. Large-kernel networks

Large-kernel networks have garnered significant attention in recent years due to their ability to capture strong inductive biases and provide large effective receptive fields [34], [46], [50], [52], [61], [83], [84], which have shown outstanding performance in visual recognition tasks. This has demonstrated that there is no inherent superiority or disadvantage between CNN and ViT architectures [34]. A series of works have focused on reducing the complexity of large-kernel convolutions [50], [61], [83], [84], enabling them to run efficiently on high-resolution feature maps. Works such as LSKNet [85], [86], LCRNet [51], UniRepLKNet [34] and SSR-STFNet [87] have shown significant advantages across various downstream tasks, establishing new SOTA results.

In contrast to prior works, we aim to enhance the effectiveness of vision foundation models in complex scenarios by introducing shape-biased representations into side-tuning through a large-kernel attention mechanism. Our proposed shape-enhanced large-kernel attention is developed under the principle of “less is more”. It builds upon proven architectural strategies while explicitly satisfying the three identified design criteria—namely, large effective receptive fields, multi-order feature interactions, and sparse connectivity. The overall design is intentionally streamlined to minimize unnecessary complexity, thereby reducing interpretive noise and facilitating a clear understanding of the core contribution.

III. RETHINKING FINE-TUNING FOR VISION: BEYOND THE NLP-INSPIRED PARADIGM

Recent advances in vision foundation models have been strongly influenced by fine-tuning paradigms from NLP [17]. In NLP, PEFT methods typically focus on storing domain-specific knowledge within a small set of trainable parameters, while relying on attention mechanisms to capture contextual dependencies. This approach is highly effective because language is a human-constructed semantic system—task-relevant

knowledge is inherently embedded in linguistic structure, and minimal adaptation often yields strong generalization.

However, vision tasks pose fundamentally different challenges. Images are objective projections of the physical world, where semantically meaningful information is often sparse and entangled with irrelevant visual signals [62]. Moreover, unlike language, the semantics of visual data are **task-defined** rather than **intrinsically encoded**, meaning the importance of features depends on the downstream task. This discrepancy makes traditional PEFT objectives—focused solely on parameter, memory, and training efficiency—insufficient for vision applications. The relatively limited success of self-supervised pretraining in vision, in contrast to its breakthroughs in NLP [13], [88], further underscores the absence of a universal representation across diverse visual tasks.

To bridge this gap, we introduce the concept of **representation efficiency** as a complementary dimension to traditional metrics in vision-specific PEFT. We refer to the efficient fine-tuning of parameters at this stage as **Vision-Centric Representation-Efficient Fine-Tuning**. Notably, this concept naturally aligns with the **Information Bottleneck (IB) theory** [68], which provides a theoretical framework for understanding efficient representations. Accordingly, we define it as follows:

Definition 1 (Representation Efficiency). Let \mathbf{x} denote an input image, and \mathbf{y} be a task-specific label (e.g., a segmentation mask). Given an intermediate representation $f(\mathbf{x})$ produced by a model, its representation efficiency $\mathcal{E}_{\text{repr}}$ is defined as:

$$\mathcal{E}_{\text{repr}}(f) = I(f(\mathbf{x}); \mathbf{y}) - \lambda I(f(\mathbf{x}); \mathbf{x}) \quad (1)$$

where $I(\cdot; \cdot)$ denotes mutual information [89] and $\lambda > 0$ is a regularization weight. This formulation promotes representations that:

- Maximize relevance to the downstream task ($I(f(\mathbf{x}); \mathbf{y})$),
- Minimize redundancy or overdependence on raw input ($I(f(\mathbf{x}); \mathbf{x})$).

This reflects the principle that effective representations should retain only task-relevant structures while suppressing noise and irrelevant details. Eq. (1) further provides a basis for designing task-specific loss functions [68]. Unlike language, where semantic priors are intrinsic, vision often requires explicit structural induction—particularly under challenging conditions such as camouflage, low texture, or noisy modalities (e.g., infrared). Different vision tasks also favor distinct representation types: salient object detection relies on texture sensitivity [90], whereas infrared small target detection depends on shape due to minimal texture cues [8], [47], [48], [82]. Thus, no single representation is universally optimal [91], and general-purpose PEFT strategies, typically built on NLP assumptions, fail to capture such task-specific variability.

We posit that optimizing for representation efficiency offers a principled direction to address this limitation. In the following sections, we present a parameter-efficient fine-tuning framework that enhances representation efficiency by explicitly introducing shape bias into the model’s inductive priors, thereby mitigating the inherent texture bias. This enables the model to achieve improved robustness in complex scenarios, while also delivering performance gains in tasks that rely heavily on texture analysis.

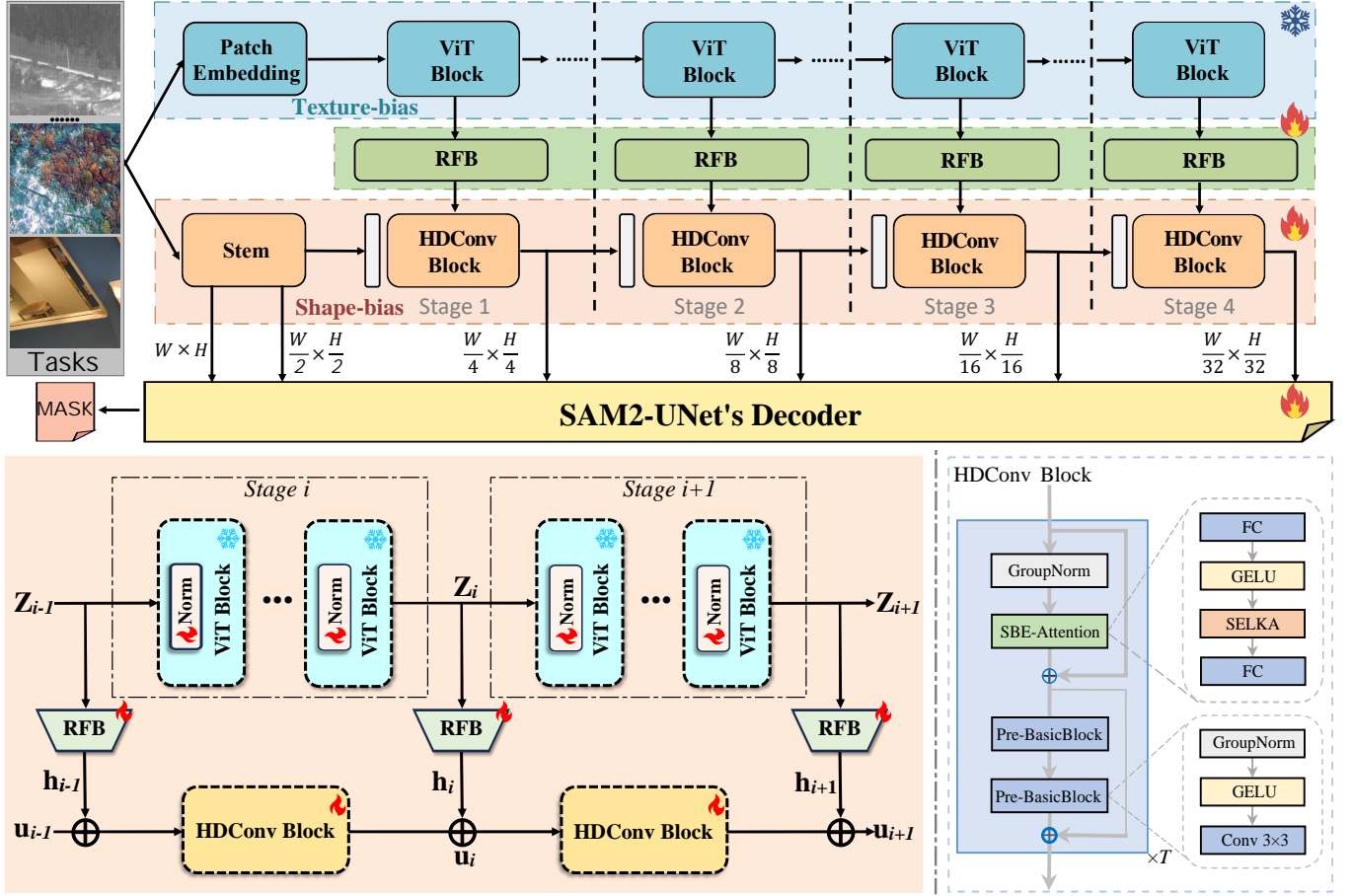


Fig. 1. Our method is developed based on the SAM2-UNet framework [18], preserving its architectural structure and design components, including the Receptive Field Block (RFB) and a decoder built from stacked DoubleConv blocks. Following the fine-tuning protocol of HST [74], we freeze most backbone parameters and update only the LayerNorm layers. All original hyperparameter settings are retained for fair comparison and reproducibility. The total number of trainable parameters in our model is 4.719M.

IV. PROPOSED METHOD

As shown in Fig. 1, the overall framework consists of two key components: Section IV-A details the proposed LSR-ST, while Section IV-B further describes the Shape-enhanced Large-kernel Attention Mechanism.

A. Ladder Shape-bias Representation Side-tuning

The overall framework of our method, shown in Fig. 1, is evaluated using SAM2-UNet [18] as the base model. SAM2-UNet performs well across various segmentation tasks but experiences performance degradation in complex scenarios, such as camouflaged and texture-weak environments, making it an ideal baseline. By replacing the original parameter-efficient fine-tuning strategy while keeping all hyperparameters fixed, we isolate the impact of our approach. The Ladder Shape-bias Representation Side-tuning (LSR-ST) structure, depicted in Fig. 1, integrates the HDConv Block into the side network to capture shape-biased representations, enhancing structural perception while maintaining parameter efficiency.

Overview of proposed LSR-ST. For the backbone [11], we fine-tune only the normalization layers, while the dimensionality reduction in the Ladder side-tuning [65] is

performed by the BRF module of SAM2-UNet [18], retaining the same hyperparameters as the baseline. The number of channels at all stages is reduced to 64. In the side network branch, the feature maps are first downsampled using the stem, followed by the proposed HDConv Block to capture shape-biased representations. Feature maps are then received and output only once at the final stage of each backbone stage. For two input feature maps, the backbone feature map $\mathbf{Z}_{i-1} \in \mathbb{R}^{W_{i-1} \times H_{i-1} \times C_{i-1}}$ and the side-network feature map $\mathbf{u}_{i-1} \in \mathbb{R}^{W_{i-1} \times H_{i-1} \times 64}$, the processing procedure can be expressed as:

$$\mathbf{u}_i = \text{HDConvBlock}(\mathbf{u}_{i-1}) + \text{RFB}(\text{VITStage}_i(\mathbf{Z}_{i-1})), \quad (2)$$

where, i denotes the i -th stage, and VITStage_i refers to the i -th stage of the frozen backbone.

The proposed HDConv Block. The structure of the HDConvBlock is shown in Fig. 1. It leverages a detail-oriented MetaFormer architecture [92], [93] designed to capture richer feature representations [51]. The block incorporates a shape-enhanced large-kernel attention mechanism as a token mixer, specifically aimed at capturing shape-biased representations. For an input feature map $\mathbf{X} \in \mathbb{R}^{W \times H \times C}$, the processing

procedure can be expressed as:

$$\mathbf{X}' = \mathbf{X} + \lambda_1 \text{SBE-Attention}(\text{GroupNorm}(\mathbf{X})), \quad (3)$$

where $\text{GroupNorm}(\cdot)$ denotes Group Normalization [94], $\text{SBE-Attention}(\cdot)$ denotes proposed shape enhanced large kernel attention. λ_1 is learnable parameter in the LayerScale [95] mechanism.

The channel mixer is implemented using a pre-activation residual block [67], which serves to store domain-specific knowledge [96] and facilitate adaptation to downstream tasks. For an input feature map $\mathbf{X}' \in \mathbb{R}^{W \times H \times C}$, the processing procedure can be expressed as:

$$\mathbf{X}'' = \mathbf{X}' + \lambda_2 \text{Pre-BasicBlock}(\text{Pre-BasicBlock}(\mathbf{X}')). \quad (4)$$

where λ_2 is also learnable parameter in the LayerScale [95] mechanism.

Advantages. Compared to adapter-based methods [17], side-tuning offers greater efficiency and decoupling, facilitating the introduction of specific representational capabilities. Unlike ViT-Adapter [97], our approach reduces memory overhead by limiting interactions with the backbone, while improving downstream performance through shape-bias representations. In contrast to LST [65] and HST [74], the HDConv Block provides superior representational capacity for handling complex scenarios. Unlike LSA [75], our method (1) employs a low-complexity large-kernel attention mechanism that is well-suited for high-resolution features, thus mitigating out-of-memory (OOM) issues; (2) leverages large-kernel convolutions, which are more effective in capturing shape bias than ViT-style attention [34]; and (3) integrates both token and channel mixers in the proposed HDConv Block, whereas LSA [75] relies solely on token mixers. Given that token mixers primarily function as feature selectors and discriminators, and channel mixers are adept at storing domain-specific knowledge [96], our architectural design significantly enhances the model's capacity to capture task-relevant information.

B. Shape Enhanced Large-kernel Attention Mechanism

The structure of the proposed Shape-Enhanced Large-Kernel Attention (SELKA) mechanism is illustrated in Fig. 2, where it functions as the central component of the SBE-Attention module illustrated in Fig.1. It follows the **design principle of “less is more”**, aiming to minimize unnecessary design complexity to enhance interpretability. Built upon the successful design of large-kernel attention mechanisms [50], [51], [61], [84], [87], [98], SELKA incorporates three key conditions—large effective receptive fields, multi-order feature interactions, and sparse connections—to enable the capture of shape-bias representations.

Overview of the proposed attention. The proposed attention mechanism follows a similar structure to MogaNet [52], LCRNet [51], and Conv2Former [98]. For an input feature map $\mathbf{X} \in \mathbb{R}^{W \times H \times C}$, the attention mechanism computes the similarity score matrix $\mathbf{A} \in \mathbb{R}^{W \times H \times C}$ and the value matrix $\mathbf{V} \in \mathbb{R}^{W \times H \times C}$. Then, it uses the Hadamard product to calculate the output $\mathbf{Z} \in \mathbb{R}^{W \times H \times C}$. The entire process is as follows:

$$\mathbf{Z} = \text{SiLU}(\mathbf{A}) \odot \text{SiLU}(\mathbf{V}), \quad (5)$$

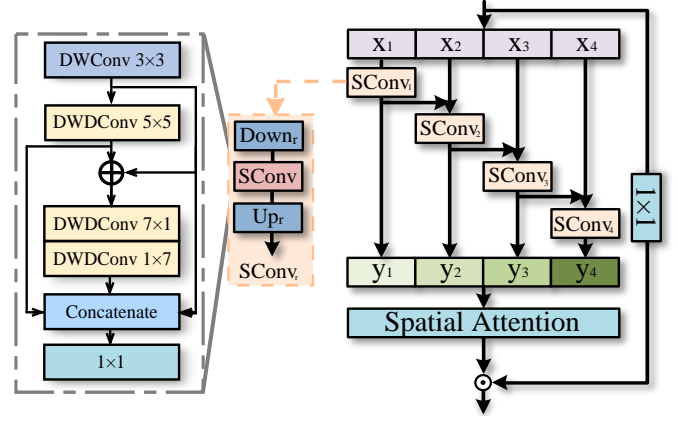


Fig. 2. The overall architecture of the proposed attention mechanism adheres to the “less is more” design philosophy, aiming to minimize unnecessary complexity while maximizing representational efficiency. It incorporates the three key conditions identified for inducing shape-biased representations—namely, a large effective receptive field, multi-order feature interactions, and sparse connections. Furthermore, by leveraging multi-scale processing and reparameterization techniques, it achieves these benefits with minimal computational overhead.

where $\text{SiLU}(\cdot)$ is sigmoid linear unit and the value matrix \mathbf{V} is computed using a simple 1×1 convolution.

The computation of the similarity score matrix is key to the attention mechanism. First, it follows the overall structure of Res2Net [78], which introduces multi-order feature interactions [52]. Second, similar to LCRNet [51], we employ an upsampling and downsampling scheme to form a multi-scale structure, enabling the construction of a broad effective receptive field at a minimal computational cost. Additionally, akin to LSKNet [85], [86], our similarity score matrix incorporates a spatial selection mechanism, which dynamically allocates the appropriate effective receptive field based on the input. Notably, the core of the proposed attention mechanism lies in the shape-bias enhanced large-kernel convolution (SConv), which provides a large effective receptive field, inductive bias, and sparse connectivity. Additionally, SConv inherently supports multi-order feature interactions.

The proposed shape-bias enhanced large-kernel convolution.

The proposed SConv is built upon the principle of large-kernel decomposition [50], [61], enabling sparse connectivity while maintaining optimization efficiency. To mitigate information loss caused by receptive field mismatch [51] and the limited interaction order resulting from sequential stacking [52], we incorporate both residual and dense connections. Additionally, a strip-based DWDCConv module [50], [84], [87] is introduced to further expand the effective receptive field and enhance the model's ability to capture structural cues such as object boundaries.

Advantages. Compared to VAN [61] and Conv2former [98], our attention mechanism satisfies all three identified conditions for shape-biased representation—namely, large effective receptive fields, multi-order feature interactions, and sparse connectivity—while further mitigating information loss and enabling dynamic receptive field allocation. In contrast to LSKNet [85], our approach also meets the three criteria and provides stronger interaction across feature hierarchies, with

reduced representational redundancy. While both our method and LCRNet [51] fulfill the conditions for inducing shape bias, we intentionally discard the complex spatial-channel selection attention in LCRNet [51] to minimize design complexity. Instead, the proposed Strip-DWDCov offers a more efficient means of capturing edge-related structural information, with a broader and dynamically allocated effective receptive field.

V. EXPERIMENT

A. Experimental Setup

1) *Datasets*: We consider six downstream tasks and their corresponding 17 publicly available datasets. These tasks are representative foreground segmentation challenges that demand strong contextual understanding. The tasks and datasets are as follows:

- Camouflaged Object Detection: CAMO [137], COD10K [138], CHAMELEON [139], and NC4K [140].
- Salient Object Detection: DUTS-TE [141], DUT-OMRON [142], HKU-IS [143], PASCAL-S [144], and ECSSD [145].
- Infrared Small Target Detection: IRSTD-1K [8], SIRSTAUG [146], and NUDT-SIRST [125].
- Marine Animal Segmentation: MAS3K [5], and RMAS [118].
- Mirror Detection: MSD [130], and PMD [131].
- Shadow Detection: ISTD [147].

For the aforementioned datasets, we follow the same pre-processing protocols as SAM2-UNet [18], SeRankDet [128], and SADT [124].

2) *Evaluation Metrics*: We use the same evaluation metrics as the baseline [18], [128] to assess the performance across various tasks. Specifically, these metrics include IoU, nIoU, P_d ($\times 10^{-2}$), F_a ($\times 10^{-6}$), S-measure (S_α), adaptive F-measure (F_β), weighted F-measure (F_β^ω), mean E-measure (S_ϕ), mean absolute error (MAE), and Balance Error Rate (BER).

3) *Implementation Details*: For the infrared small target detection task, we use the same input size as SeRankDet [128] and employ SoftIoU Loss. The number of training epochs is kept consistent with SeRankDet [128]. When testing MDSAM [30] and SAM2-UNet [18] for infrared small target detection, we modify the training strategy and input size of MDSAM [30] and SAM2-UNet [18] to align with SeRankDet [128]. For other tasks, we keep the input size consistent with the baseline [18], which is 352×352, and use the same loss functions and training strategies as SAM2-UNet [18].

B. Comparison with State-of-the-Arts

To validate the effectiveness of the proposed method, we conduct extensive comparative experiments against previous state-of-the-art (SOTA) algorithms across six downstream tasks on 17 publicly available datasets.

1) *Quantitative Evaluation*: The evaluation results on camouflaged object detection are presented in Tab. I. Compared to SAM2-UNet [18], our method achieves consistent improvements across all metrics, demonstrating the effectiveness of LSR-ST in enhancing performance via shape-biased representation learning. Furthermore, we surpass 23 SOTA methods,

achieving the best performance on multiple benchmarks. Notably, FGSANet [23], a frequency-domain adapter-based method, lags behind our approach, highlighting the advantage of shape bias over handcrafted frequency cues.

Tab. II shows results on salient object detection, a task heavily reliant on texture and global contrast [3]. Despite the lesser importance of shape bias in this context, our method maintains parity with SAM2-UNet across all metrics, underscoring its robustness. As observed, SAM-based methods consistently perform well, reinforcing the strong generalization capabilities of foundation models.

For marine animal segmentation (Tab. III), a sub-task of camouflage detection under marine environments [5], our method achieves substantial improvements over SAM2-UNet and outperforms all nine SOTA baselines, setting a new benchmark. In shadow detection (also Tab. III), which involves ambiguous visual cues and high false-positive risks, our method delivers strong performance, ranking just below the domain-knowledge-driven RMLANet [6]. Notably, we surpass SAM2-UNet by a clear margin, validating our approach under diverse visual conditions. Infrared small target detection results are summarized in Tab. IV. This task is extremely challenging due to low signal-to-clutter ratios, limited texture, and heavy background noise. Our method outperforms all baselines across three datasets with varying characteristics, benefiting significantly from the proposed shape-biased representations, which compensate for the lack of texture by emphasizing structure. Finally, in mirror detection (Tab. V), which requires modeling complex semantics between real and reflected objects, our method achieves SOTA performance, particularly on the challenging PMD dataset, demonstrating strong capability in complex reasoning scenarios.

In summary, across six downstream tasks and 17 publicly available datasets, our method consistently outperforms SAM2-UNet [18]. The gains are especially pronounced in structurally complex scenarios, while performance is maintained in texture-dominated tasks, confirming the generality and robustness of our shape-biased representation strategy.

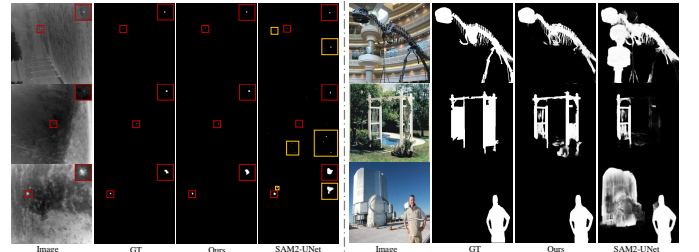


Fig. 3. Visualization comparison of detection results via Infrared small target detection and salient object detection. It can be observed that in complex textured backgrounds, SAM2-UNet [18] suffers from significant false positives due to texture bias. In contrast, by introducing shape bias, our method effectively adapts to the infrared small target detection task. Moreover, for salient object detection tasks that rely heavily on texture information, our approach also achieves notable improvements.

2) *Qualitative Evaluation*: To intuitively demonstrate the advantages of the proposed method, we present the qualitative results of the experiments, as shown in Fig. 3 and Fig. 4.

TABLE I

COMPARISON WITH SOTA METHODS ON CAMOUFLAGED OBJECT DETECTION. THE BEST AND SECOND RESULTS ARE IN **RED** AND **BLUE**, RESPECTIVELY.

Method	Publish	CHAMELEON (N=76)				CAMO (N=250)				COD10K (N=2026)				NC4K (N=4121)			
		$S_\alpha \uparrow$	$E_\phi \uparrow$	$F_\beta^\omega \uparrow$	$M \downarrow$	$S_\alpha \uparrow$	$E_\phi \uparrow$	$F_\beta^\omega \uparrow$	$M \downarrow$	$S_\alpha \uparrow$	$E_\phi \uparrow$	$F_\beta^\omega \uparrow$	$M \downarrow$	$S_\alpha \uparrow$	$E_\phi \uparrow$	$F_\beta^\omega \uparrow$	$M \downarrow$
Task-specific Proprietary Methods																	
SARNe [99]	TCSVT'23	.933	.978	.909	.017	.874	.935	.844	.046	.885	.947	.820	.021	.889	.940	.851	.032
FSPNe [100]	CVPR'23	.908	.965	.851	.023	.856	.928	.799	.050	.851	.930	.735	.026	.878	.937	.816	.035
MSCAFNe [69]	TCSVT'23	.912	.970	.865	.022	.873	.937	.828	.046	.865	.936	.776	.024	.887	.942	.838	.032
HitNet [101]	AAAI'23	.921	.972	.897	.019	.849	.910	.809	.055	.871	.938	.806	.023	.875	.929	.834	.037
Yang <i>et al.</i> [102]	TCSVT'24	.906	.966	.888	.024	.835	.902	.828	.063	.834	.912	.778	.030	.859	.922	.843	.041
Liu <i>et al.</i> [103]	TCSVT'24	-	-	-	-	.886	.939	.854	.040	.881	.933	.803	.022	.899	.945	.854	.028
Wang <i>et al.</i> [104]	TCSVT'24	.918	.959	.880	.019	.868	.925	.832	.047	.869	.936	.792	.023	.887	.939	.846	.031
MVGNet [105]	TCSVT'24	.922	.969	.882	.019	.879	.930	.839	.045	.877	.936	.799	.022	.894	.938	.850	.030
CamoFormer [106]	TPAMI'24	-	-	-	-	.878	.934	.839	.044	.872	.934	.793	.022	.893	.940	.850	.030
RISNet [107]	CVPR'24	-	-	-	-	.870	.922	.827	.050	.873	.931	.799	.025	.882	.925	.834	.037
HGINet [108]	TIP'24	-	-	-	-	.874	.937	.848	.041	.882	.949	.821	.019	.894	.947	.865	.027
SENet [109]	TIP'25	.918	.957	.878	.019	.888	.932	.847	.039	.865	.925	.780	.024	.889	.933	.843	.032
PRBE-Net [81]	TMM'25	.918	.951	.878	.020	.876	.928	.837	.045	.867	.932	.793	.021	.887	.931	.845	.031
AdaptCOD [9]	IJCV'25	-	-	-	-	.886	.932	-	.043	.892	.938	-	.021	.906	.942	-	.029
Diffusion Model for Camouflaged Object Detection																	
PrObE [110]	NIPS'23	-	-	-	-	.797	.871	.702	.071	.803	.869	.661	.037	.838	.900	.755	.049
FocusDiffuser-P [70]	ECCV'24	-	-	-	-	.881	.939	.851	.042	.875	.939	.809	.020	.891	.940	.854	.029
UGDNet [111]	TMM'25	.922	.970	.892	.018	.888	.942	.865	.038	.885	.947	.822	.019	.895	.943	.862	.028
CamoDiffusion [112]	TPAMI'25	-	-	-	-	.878	.940	.853	.042	.881	.944	.814	.020	.893	.942	.859	.029
Segment Anything Model for Camouflaged Object Detection																	
SAM [10]	ICCV'23	.767	.776	.696	.078	.684	.687	.606	.132	.783	.798	.701	.050	.767	.776	.696	.078
SAM-Adapter [113]	ICCVW'23	.896	.919	.824	.033	.847	.873	.765	.070	.883	.918	.801	.025	-	-	-	-
SAM2-UNet [18]	ARXIV'24	.914	.961	.863	.022	.884	.932	.861	.042	.880	.936	.789	.021	.901	.941	.863	.029
FGSAnet [23]	TMM'25	.915	.969	.901	.017	.873	.938	.853	.043	.889	.936	.839	.018	.893	.934	.865	.027
Ours	-	.930	.965	.901	.016	.901	.942	.872	.035	.897	.948	.837	.017	.908	.945	.873	.026

TABLE II

COMPARISON WITH SOTA METHODS ON SALIENT OBJECT DETECTION. THE BEST AND SECOND RESULTS ARE IN **RED** AND **BLUE**, RESPECTIVELY.

Method	DUTS-TE (N=5019)				DUT-OMRON (N=5618)				HKU-IS (N=4447)				ECSSD (N=1000)				PASCAL-S (N=850)			
	$S_\alpha \uparrow$	$E_\phi \uparrow$	$F_\beta^m \uparrow$	$M \downarrow$	$S_\alpha \uparrow$	$E_\phi \uparrow$	$F_\beta^m \uparrow$	$M \downarrow$	$S_\alpha \uparrow$	$E_\phi \uparrow$	$F_\beta^m \uparrow$	$M \downarrow$	$S_\alpha \uparrow$	$E_\phi \uparrow$	$F_\beta^m \uparrow$	$M \downarrow$	$S_\alpha \uparrow$	$E_\phi \uparrow$	$F_\beta^m \uparrow$	$M \downarrow$
PDRNet ₂₂ [114]	.877	-	.845	.035	.846	-	.756	.052	.924	-	.911	.027	.927	-	.920	.032	.865	-	.816	.061
TCRNet ₂₃ [115]	.880	-	.842	.034	.843	-	.748	.054	.923	-	.908	.026	.928	-	.917	.031	.865	-	.817	.059
BBRF ₂₃ [71]	.908	.927	.916	.025	.855	.887	.843	.042	.935	.965	.958	.020	.939	.934	.963	.022	.871	.867	.891	.049
MENet ₂₃ [90]	.905	.938	.918	.028	.850	.871	.845	.045	.927	.960	.951	.023	.928	.951	.957	.021	.872	.910	.897	.053
EVPv ₁₂₃ [1]	.913	.947	.923	.026	.862	.894	.858	.046	.931	.961	.952	.024	.935	.957	.960	.027	.878	.917	.872	.054
EVPv ₂₂₃ [19]	.915	.948	.923	.027	.862	.895	.857	.047	.932	.963	.953	.023	.935	.957	.958	.028	.879	.917	.869	.053
MDSAM ₂₄ [30]	.920	.949	.937	.024	.878	.910	.887	.039	.941	.969	.963	.019	.948	.967	.974	.021	.882	.917	.907	.052
ADMNet ₂₄ [116]	.849	.893	.813	.052	.826	.869	.763	.058	.901	.946	.906	.036	.900	.933	.909	.049	.815	.862	.796	.088
SAM2-UNet ₂₄ [18]	.934	.959	-	.020	.884	.912	-	.039	.941	.971	-	.019	.950	.970	-	.020	.894	.931	-	.043
Ours	.936	.961	.920	.019	.893	.923	.846	.033	.944	.971	.941	.018	.954	.971	.951	.018	.897	.932	.872	.042

TABLE III

COMPARISON ON MARINE ANIMAL SEGMENTATION AND SHADOW DETECTION. THE BEST AND SECOND RESULTS ARE IN **RED** AND **BLUE**, RESPECTIVELY.

Method	Publish	MAS3K					RMAS					Method	ISTD BER \downarrow
		mIoU \uparrow	$S_\alpha \uparrow$	$F_\beta^w \uparrow$	$E_\phi \uparrow$	MAE \downarrow	mIoU \uparrow	$S_\alpha \uparrow$	$F_\beta^w \uparrow$	$E_\phi \uparrow$	MAE \downarrow		
ECDNet [5]	TCSVT'21	0.711	0.850	0.766	0.901	0.036	0.664	0.823	0.689	0.854	0.036	EVPv ₁₂₃ [1]	1.35
OCENet [117]	WACV'22	0.667	0.824	0.703	0.868	0.052	0.680	0.836	0.752	0.900	0.030	EVPv ₂₂₃ [19]	1.35
ZoomNet [2]	CVPR'22	0.736	0.862	0.780	0.898	0.032	0.728	0.855	0.795	0.915	0.022	SDTR ₂₃ [122]	1.51
MASNet [118]	J-OE'23	0.742	0.864	0.788	0.906	0.032	0.731	0.862	0.801	0.920	0.024	ShadowSAM ₂₃ [123]	1.36
SAM [10]	ICCV'23	0.566	0.763	0.656	0.807	0.059	0.445	0.697	0.534	0.790	0.053	RMLANet ₂₃ [6]	1.01
SAM-Ad [119]	ICCVW'23	0.714	0.847	0.782	0.914	0.033	0.656	0.816	0.752	0.927	0.027	SADT ₂₄ [124]	1.05
SAM-DA [120]	ARXIV'23	0.742	0.866	0.806	0.925	0.028	0.686	0.833	0.780	0.926	0.024	TS-SAM ₂₄ [22]	1.04
Dual-SAM [121]	CVPR'24	0.789	0.884	0.838	0.933	0.023	0.735	0.860	0.812	0.944	0.022	SAM2-UNet ₂₄ [18]	1.62
SAM2-UNet [18]	ARXIV'24	0.799	0.903	0.848	0.943	0.021	0.738	0.874	0.810	0.944	0.022	Ours	0.93
Ours	-	0.822	0.911	0.869	0.950	0.020	0.760	0.880	0.829	0.953	0.021		

TABLE IV
COMPARISON WITH OTHER SOTA METHODS ON THREE DATASETS. THE BEST AND SECOND RESULTS ARE IN **RED** AND **BLUE**, RESPECTIVELY.

Method	Publish	Param	IRSTD-1k				SIRSTAUG				NUDT-SIRST			
			IoU \uparrow	nIoU \uparrow	P_d \uparrow	F_a \downarrow	IoU \uparrow	nIoU \uparrow	P_d \uparrow	F_a \downarrow	IoU \uparrow	nIoU \uparrow	P_d \uparrow	F_a \downarrow
Deep Learning Methods														
DNA ^{Net} [125]	TIP'22	4.6968M	68.87	67.53	94.95	13.38	74.88	70.23	97.8	30.07	92.67	92.09	99.53	2.347
IS ^{Net} [8]	CVPR'22	1.09M	68.77	64.84	95.56	15.39	72.50	70.84	98.41	28.61	89.81	88.92	99.12	4.211
UIU ^{Net} [126]	TIP'23	50.54M	69.13	67.19	94.27	16.47	74.24	70.57	98.35	23.13	90.77	90.17	99.29	2.39
MTU ^{Net} [127]	TGRS'23	4.07M	67.50	66.15	93.27	14.75	74.70	70.66	98.49	39.73	87.49	87.70	98.60	3.76
SeRank ^{Det} [128]	TGRS'24	108.89M	73.66	69.11	94.28	8.37	75.49	71.08	98.97	18.90	94.28	93.69	99.77	2.03
MSH ^{Net} [129]	CVPR'24	4.07M	67.87	61.70	92.86	8.88	-	-	-	-	80.55	-	97.99	11.77
CSR ^{Net} [47]	TIP'24	0.4045M	65.87	66.70	98.16	12.08	-	-	-	-	-	-	-	-
Fine-tuning Models Based on Segment Anything Model [10]														
IR ^{SAM} [14]	ECCV'24	12.33M	73.69	68.97	96.92	7.55	-	-	-	-	92.59	93.29	98.87	6.94
MDS ^{AM} [30]	MM'24	-	60.82	62.12	93.60	19.04	76.51	73.13	99.86	5.07	89.22	92.50	99.35	10.76
SAM2-UN ^{et} [18]	ARXIV'24	4.269M	67.10	62.87	93.93	3.20	74.35	71.32	99.86	3.22	70.51	75.18	98.30	4.31
Ours	-	4.719M	74.78	69.73	98.10	1.3	75.79	74.23	99.81	4.77	96.76	96.43	99.58	2.03

TABLE V
COMPARISON WITH SOTA METHODS ON MIRROR DETECTION. THE BEST AND SECOND RESULTS ARE IN **RED** AND **BLUE**, RESPECTIVELY.

Method	Publish	PMD					MSD				
		IoU \uparrow	Acc \uparrow	F_β \uparrow	MAE \downarrow	BER \downarrow	IoU \uparrow	Acc \uparrow	F_β \uparrow	MAE \downarrow	BER \downarrow
MirrorNet [130]	ICCV'19	58.51	70.18	0.741	0.043	15.61	78.95	93.29	0.857	0.065	6.39
PMDNet [131]	CVPR'20	66.00	77.15	0.785	0.033	12.13	81.55	88.20	0.892	0.047	7.17
VST [132]	ICCV'21	59.06	-	0.769	0.035	-	79.09	-	0.867	0.052	-
SANet [133]	CVPR'22	66.84	74.98	0.795	0.071	13.44	79.85	86.69	0.877	0.054	8.31
VCNet [134]	TPAMI'22	64.02	69.26	0.811	0.035	15.68	80.08	85.53	0.897	0.048	8.43
SATNet [135]	AAAI'23	69.38	77.22	0.847	0.025	11.93	85.41	89.14	0.922	0.033	6.21
CSFwinformer [4]	TIP'24	70.05	78.27	0.838	0.024	11.41	82.08	88.92	0.896	0.045	7.14
DPRNet [136]	TCSVT'24	72.10	-	-	0.026	-	86.60	-	-	0.033	-
SAM2-UNet [18]	ARXIV'24	72.80	-	-	0.027	-	91.80	-	-	0.027	-
Ours	-	79.25	89.94	0.826	0.018	5.80	92.43	96.86	0.907	0.021	2.55

From the qualitative results, it is evident that the proposed method demonstrates robustness across various scenarios. In the mirror detection task, the proposed method outperforms SAM2-UNet [18] and CSFwinformer [4] by accurately distinguishing between objects inside and outside the mirror, while also focusing on the fine details of the mirror image. This is due to the presence of shape-bias representation, which allows the model to analyze the relationships between objects or parts of objects in the scene, thus effectively differentiating between real objects and their reflections. In the shadow detection task, the proposed method excels at understanding the scene context, particularly when the scene contains complex textures. In such cases, SAM2-UNet [18], SADT [122], PMLANet [6], and EVPv2 [19] fail to correctly handle the complex textured areas in the background, producing erroneous responses. In contrast, our method, which incorporates shape-bias representation, accurately detects shadows while minimizing false responses. In camouflage target detection scenarios, where the texture of the target closely matches that of the background, the proposed method, by incorporating shape-bias representation, demonstrates significantly stronger robustness. The shape-bias representation allows the model to focus on the structural features of the target, enabling it to distinguish subtle differences between the target and the background, even when texture cues are highly consistent. This enhances the model's ability to

detect camouflaged targets, even in challenging environments where traditional texture-based approaches may struggle.

C. Ablation Study

In this section, we focus on discussing the effectiveness of incorporating shape-bias representations into side-tuning. To this end, we perform the following ablation experiments:

- (1) HDConv Block w/o Large-Kernel Attention Mechanism Token Mixer
- (2) HDConv Block w/ LKA [61] Large-Kernel Attention Mechanism Token Mixer
- (3) HDConv Block w/ LSKA [50] Large-Kernel Attention Mechanism Token Mixer
- (4) HDConv Block w/ ConvMod [98] Large-Kernel Attention Mechanism Token Mixer
- (5) HDConv Block w/ SMixer [52] Large-Kernel Attention Mechanism Token Mixer
- (6) HDConv Block w/ DLC-Attention [51] Large-Kernel Attention Mechanism Token Mixer

where: (1) represents the simple Ladder Side-tuning [65], which lacks shape-bias representation capability; (2) represents a model with sparse connections and a large effective receptive field, but lacking multi-scale feature interactions and prone to information loss; (4) represents a model with a large effective

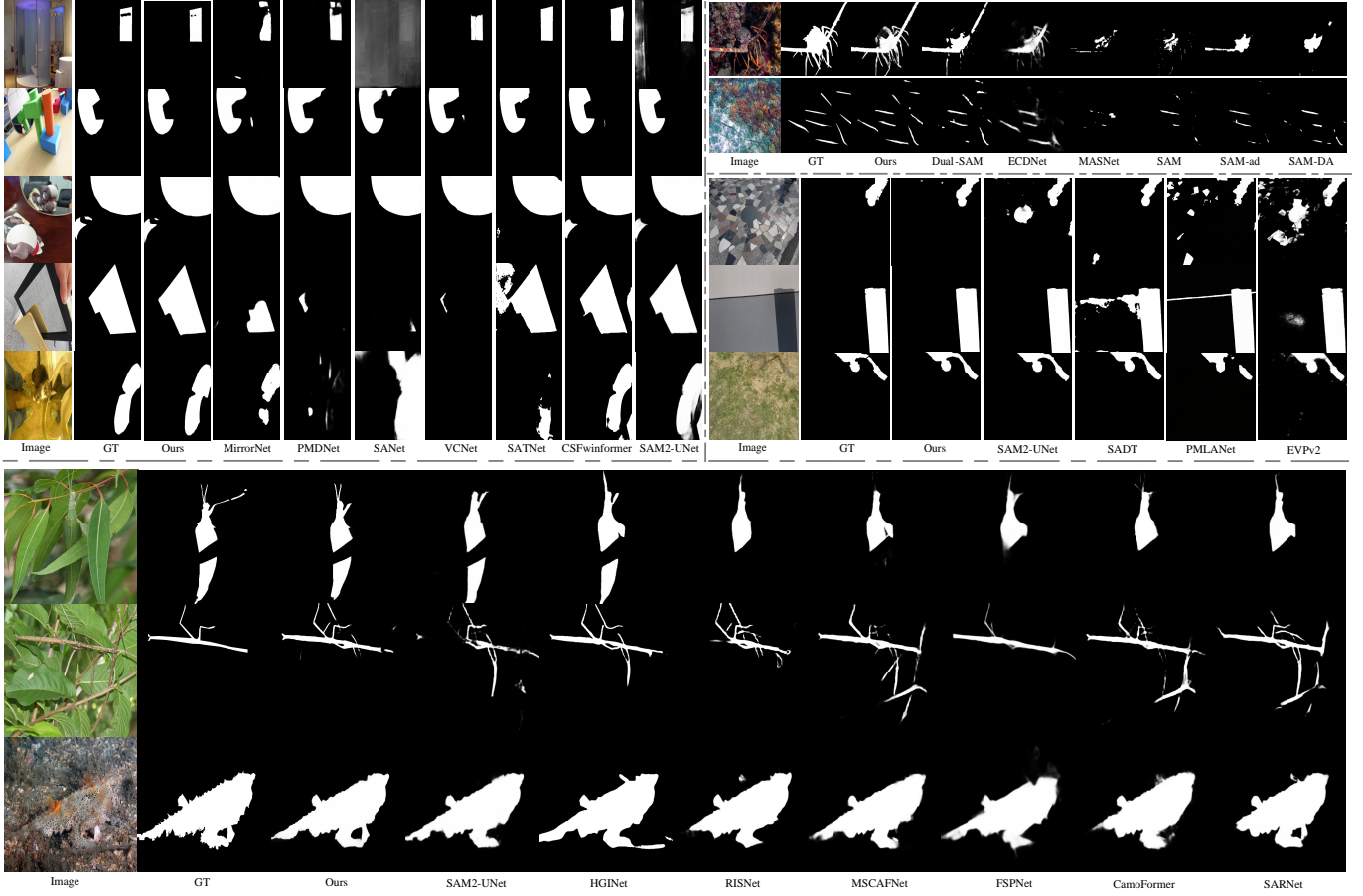


Fig. 4. Visualization comparison of detection results via different tasks.

TABLE VI
ABLATION STUDY ON CAMOUFLAGED OBJECT DETECTION. THE BEST AND SECOND RESULTS ARE IN **RED** AND **BLUE**, RESPECTIVELY.

Method	Publish	CHAMELEON (N=76)				CAMO (N=250)				COD10K (N=2026)				NC4K (N=4121)			
		$S_\alpha \uparrow$	$E_\phi \uparrow$	$F_\beta^\omega \uparrow$	$M \downarrow$	$S_\alpha \uparrow$	$E_\phi \uparrow$	$F_\beta^\omega \uparrow$	$M \downarrow$	$S_\alpha \uparrow$	$E_\phi \uparrow$	$F_\beta^\omega \uparrow$	$M \downarrow$	$S_\alpha \uparrow$	$E_\phi \uparrow$	$F_\beta^\omega \uparrow$	$M \downarrow$
Baseline																	
SAM2-UNet [18]	ARXIV'24	.914	.961	.863	.022	.884	.932	.861	.042	.880	.936	.789	.021	.901	.941	.863	.029
Conventional Advanced Adapters																	
LMSA [30]	MM'24	.917	.961	.871	.020	.886	.928	.845	.042	.882	.934	.802	.021	.903	.941	.861	.029
Mona [148]	CVPR'25	.920	.964	.875	.020	.885	.930	.847	.042	.883	.937	.805	.021	.902	.940	.858	.029
Ablation Conditions: Conditions for the Emergence of Shape Bias																	
Condition (1) [65]	NIPS'22	.754	.845	.617	.071	.659	.745	.508	.131	.690	.766	.486	.070	.721	.793	.580	.094
Condition (2) [61]	CVMJ'23	.926	.964	.893	.016	.889	.936	.859	.038	.892	.940	.828	.018	.902	.940	.867	.027
Condition (3) [50]	ESA'24	.926	.963	.893	.016	.888	.934	.860	.039	.892	.939	.827	.018	.902	.941	.867	.027
Condition (4) [98]	TPAMI'24	.923	.963	.888	.017	.887	.934	.857	.038	.889	.936	.822	.018	.902	.940	.866	.027
Condition (5) [52]	ICLR'24	.925	.962	.889	.016	.887	.931	.856	.039	.892	.938	.826	.018	.903	.941	.867	.027
Condition (6) [51]	ARXIV'24	.924	.962	.889	.018	.892	.937	.859	.040	.896	.948	.836	.018	.908	.944	.872	.027
Ours	-	.930	.965	.901	.016	.901	.942	.872	.035	.897	.948	.837	.017	.908	.945	.873	.026

receptive field and partial multi-scale feature interactions, but suffers from information loss and lacks sparse connections; (5) represents a model with a large effective receptive field, multi-scale feature interactions, and sparse connections, but unable to dynamically adjust the effective receptive field, thus leading to information loss; (6) represents a model with a large effective receptive field, sparse connections, multi-scale feature interactions, and the ability to dynamically allocate the

effective receptive field, thereby mitigating information loss;

The ablation results in Tab. VI demonstrate that conventional advanced adapters fail to overcome texture bias, and therefore cannot consistently and substantially improve the baseline's performance in complex scenarios. Condition (1) performs poorly due to three factors: (i) it retains the baseline's fixed channel reduction to 64 via the RFB module, rather than scaling the original width; (ii) the removal of the token mixer

reduces HDConv to a simple residual block with limited representational capacity; and (iii) tuning is only applied at the end of each stage, rather than after every block, thereby limiting representation learning. Conditions (2)–(5) partially fulfill the three key conditions for inducing shape bias, resulting in moderate yet consistent performance drops. Both Condition (6) and our proposed method satisfy all three conditions; however, our approach further incorporates a strip-based DWDCov to implicitly enhance structure and edge awareness, thereby achieving the best overall performance.

D. Limitations

While our approach builds upon the SAM2 encoder [18], which has proven effective for many image-based tasks, it is limited in its direct applicability to temporal tasks. This is primarily due to the exclusion of motion representation learning, which remains an open challenge. A promising avenue for future work is to explore how to jointly capture appearance priors and motion information in dynamic, spatiotemporal contexts, thus extending the model’s applicability to more complex temporal and video-based tasks.

VI. CONCLUSION

In this paper, we revisited parameter-efficient fine-tuning for vision foundation models from a representation learning perspective. We identified texture bias as a key factor limiting generalization in complex visual tasks, and introduced the concept of “*representation efficiency*” to guide the design of robust fine-tuning strategies. To this end, we proposed LSR-ST, a simple yet effective framework that incorporates shape-biased representations through a lightweight HDConv Block. Extensive experiments across diverse tasks and datasets demonstrate that LSR-ST achieves strong performance in both texture-sensitive and structure-dependent scenarios, using only 4.719M trainable parameters. Our findings offer new insights into the role of inductive biases in vision adaptation and suggest promising directions for future work in efficient model tuning.

REFERENCES

- [1] W. Liu, X. Shen, C.-M. Pun, and X. Cun, “Explicit visual prompting for low-level structure segmentations,” in *Proceedings of the IEEE/CVF Conference on Computer Vision and Pattern Recognition*, 2023, pp. 19 434–19 445.
- [2] Y. Pang, X. Zhao, T.-Z. Xiang, L. Zhang, and H. Lu, “Zoom in and out: A mixed-scale triplet network for camouflaged object detection,” in *CVPR*, 2022, pp. 2160–2170.
- [3] J.-J. Liu, Q. Hou, M.-M. Cheng, J. Feng, and J. Jiang, “A simple pooling-based design for real-time salient object detection,” in *Proceedings of the Conference on Computer Vision and Pattern Recognition (CVPR)*, 2019.
- [4] Z. Xie, S. Wang, Q. Yu, X. Tan, and Y. Xie, “Csfwinformer: Cross-space-frequency window transformer for mirror detection,” *IEEE Transactions on Image Processing*, 2024.
- [5] L. Li, B. Dong, E. Rigall, T. Zhou, J. Dong, and G. Chen, “Marine animal segmentation,” *TCSVT*, vol. 32, no. 4, pp. 2303–2314, 2021.
- [6] L. Jie and H. Zhang, “Rmlanet: Random multi-level attention network for shadow detection and removal,” *IEEE Transactions on Circuits and Systems for Video Technology*, vol. 33, no. 12, pp. 7819–7831, 2023.
- [7] S. Chen, H. Wang, Z. Shen, G. Zhang, C. Ning, and X. Zhang, “A feature enhancement and augmentation-based infrared small target detection network,” *IEEE Geoscience and Remote Sensing Letters*, vol. 21, pp. 1–5, 2024.
- [8] M. Zhang, R. Zhang, Y. Yang, H. Bai, J. Zhang, and J. Guo, “Isnet: Shape matters for infrared small target detection,” in *2022 IEEE/CVF Conference on Computer Vision and Pattern Recognition (CVPR)*, 2022, pp. 867–876.
- [9] B. Yin, X. Zhang, L. Liu, M.-M. Cheng, Y. Liu, and Q. Hou, “Camouflaged object detection with adaptive partition and background retrieval,” *International Journal of Computer Vision*, pp. 1–17, 2025.
- [10] A. Kirillov, E. Mintun, N. Ravi, H. Mao, C. Rolland, L. Gustafson, T. Xiao, S. Whitehead, A. C. Berg, W.-Y. Lo, P. Dollár, and R. Girshick, “Segment anything,” in *2023 IEEE/CVF International Conference on Computer Vision (ICCV)*, 2023, pp. 3992–4003.
- [11] N. Ravi, V. Gabeur, Y.-T. Hu, R. Hu, C. Ryali, T. Ma, H. Khedr, R. Rädle, C. Rolland, L. Gustafson *et al.*, “Sam 2: Segment anything in images and videos,” *arXiv preprint arXiv:2408.00714*, 2024.
- [12] M. Oquab, T. Darcet, T. Moutakanni, H. Vo, M. Szafraniec, V. Khalidov, P. Fernandez, D. Haziza, F. Massa, A. El-Nouby *et al.*, “Dinov2: Learning robust visual features without supervision,” *arXiv preprint arXiv:2304.07193*, 2023.
- [13] A. Radford, J. W. Kim, C. Hallacy, A. Ramesh, G. Goh, S. Agarwal, G. Sastry, A. Askell, P. Mishkin, J. Clark *et al.*, “Learning transferable visual models from natural language supervision,” in *International conference on machine learning*. PmlR, 2021, pp. 8748–8763.
- [14] M. Zhang, Y. Wang, J. Guo, Y. Li, X. Gao, and J. Zhang, “Irsam: Advancing segment anything model for infrared small target detection,” in *Computer Vision – ECCV 2024*. Cham: Springer Nature Switzerland, 2025, pp. 233–249.
- [15] Y. Xu, J. Tang, A. Men, and Q. Chen, “Eviprompt: A training-free evidential prompt generation method for adapting segment anything model in medical images,” *IEEE Transactions on Image Processing*, vol. 33, pp. 6204–6215, 2024.
- [16] X. Wei, J. Cao, Y. Jin, M. Lu, G. Wang, and S. Zhang, “I-medsam: Implicit medical image segmentation with segment anything,” in *European Conference on Computer Vision*. Springer, 2024, pp. 90–107.
- [17] Z. Han, C. Gao, J. Liu, J. Zhang, and S. Q. Zhang, “Parameter-efficient fine-tuning for large models: A comprehensive survey,” *arXiv preprint arXiv:2403.14608*, 2024.
- [18] X. Xiong, Z. Wu, S. Tan, W. Li, F. Tang, Y. Chen, S. Li, J. Ma, and G. Li, “Sam2-UNET: Segment anything 2 makes strong encoder for natural and medical image segmentation,” *arXiv preprint arXiv:2408.08870*, 2024.
- [19] W. Liu, X. Shen, C.-M. Pun, and X. Cun, “Explicit visual prompting for universal foreground segmentations,” *arXiv preprint arXiv:2305.18476*, 2023.
- [20] Z. You, L. Kong, L. Meng, and Z. Wu, “FOCUS: Towards universal foreground segmentation,” in *AAAI*, 2025.
- [21] X. Zhao, Y. Pang, L. Zhang, H. Lu, and L. Zhang, “Towards diverse binary segmentation via a simple yet general gated network,” *International Journal of Computer Vision*, vol. 132, no. 10, pp. 4157–4234, 2024.
- [22] Y. Yu, C. Xu, and K. Wang, “Ts-sam: Fine-tuning segment-anything model for downstream tasks,” in *2024 IEEE International Conference on Multimedia and Expo (ICME)*. IEEE, 2024, pp. 1–6.
- [23] S. Zhang, D. Kong, Y. Xing, Y. Lu, L. Ran, G. Liang, H. Wang, and Y. Zhang, “Frequency-guided spatial adaptation for camouflaged object detection,” *IEEE Transactions on Multimedia*, vol. 27, pp. 72–83, 2025.
- [24] Z. Huang, Z. Zhang, C. Lan, Z.-J. Zha, Y. Lu, and B. Guo, “Adaptive frequency filters as efficient global token mixers,” in *ICCV*, 2023.
- [25] T. Chen and Z. Ye, “Freqodes: Frequency neural ode networks for infrared small target detection,” *IEEE Transactions on Geoscience and Remote Sensing*, 2024.
- [26] Z. Zhou, Y. Song, M. Li, S. Hu, X. Wang, L. Y. Zhang, D. Yao, and H. Jin, “Darksam: Fooling segment anything model to segment nothing,” *Advances in Neural Information Processing Systems*, vol. 37, pp. 49 859–49 880, 2024.
- [27] C. Zhang, Y. Qiao, S. Tariq, S. Zheng, C. Zhang, C. Li, H. Shin, and C. S. Hong, “Understanding segment anything model: Sam is biased towards texture rather than shape,” *arXiv preprint arXiv:2311.11465*, 2023.
- [28] Y. Qiao, C. Zhang, T. Kang, D. Kim, C. Zhang, and C. S. Hong, “Robustness of sam: Segment anything under corruptions and beyond,” *arXiv preprint arXiv:2306.07713*, 2023.
- [29] T. Zhang, J. Wen, Z. Chen, K. Ding, S. Xiang, and C. Pan, “Unip: Rethinking pre-trained attention patterns for infrared semantic segmentation,” *arXiv preprint arXiv:2502.02257*, 2025.
- [30] S. Gao, P. Zhang, T. Yan, and H. Lu, “Multi-scale and detail-enhanced segment anything model for salient object detection,” in *Proceedings of the 32nd ACM International Conference on Multimedia*, 2024, pp. 9894–9903.

- [31] W. Tu, W. Deng, and T. Gedeon, "A closer look at the robustness of contrastive language-image pre-training (clip)," *Advances in Neural Information Processing Systems*, vol. 36, pp. 13 678–13 691, 2023.
- [32] M. Wortsman, G. Ilharco, J. W. Kim, M. Li, S. Kornblith, R. Roelofs, R. G. Lopes, H. Hajishirzi, A. Farhadi, H. Namkoong *et al.*, "Robust fine-tuning of zero-shot models," in *Proceedings of the IEEE/CVF conference on computer vision and pattern recognition*, 2022, pp. 7959–7971.
- [33] S. Sundaram, S. Fu, L. Muttenthaler, N. Tamir, L. Chai, S. Kornblith, T. Darrell, and P. Isola, "When does perceptual alignment benefit vision representations?" *Advances in Neural Information Processing Systems*, vol. 37, pp. 55 314–55 341, 2024.
- [34] X. Ding, Y. Zhang, Y. Ge, S. Zhao, L. Song, X. Yue, and Y. Shan, "Unireplknet: A universal perception large-kernel convnet for audio video point cloud time-series and image recognition," in *Proceedings of the IEEE/CVF Conference on Computer Vision and Pattern Recognition*, 2024, pp. 5513–5524.
- [35] S. Lee, I. Hwang, G.-C. Kang, and B.-T. Zhang, "Improving robustness to texture bias via shape-focused augmentation," in *Proceedings of the IEEE/CVF conference on computer vision and pattern recognition*, 2022, pp. 4323–4331.
- [36] B. Shi, D. Zhang, Q. Dai, Z. Zhu, Y. Mu, and J. Wang, "Informative dropout for robust representation learning: A shape-bias perspective," in *International Conference on Machine Learning*. PMLR, 2020, pp. 8828–8839.
- [37] J. Theodoridis, J. Hofmann, J. Maucher, and A. Schilling, "Trapped in texture bias? a large scale comparison of deep instance segmentation," in *European Conference on Computer Vision*. Springer, 2022, pp. 609–627.
- [38] X. He, Q. Lin, C. Luo, W. Xie, S. Song, F. Liu, and L. Shen, "Shift from texture-bias to shape-bias: Edge deformation-based augmentation for robust object recognition," in *Proceedings of the IEEE/CVF International Conference on Computer Vision*, 2023, pp. 1526–1535.
- [39] X. Ye, Y. Chang, R. Xu, and H. Li, "Uw-adapter: Adapting monocular depth estimation model in underwater scenes," *IEEE Transactions on Multimedia*, pp. 1–11, 2025.
- [40] X. Yang, G. Lin, Z. Chen, and L. Zhou, "Neural vector fields: Implicit representation by explicit learning," in *Proceedings of the IEEE/CVF conference on computer vision and pattern recognition*, 2023, pp. 16 727–16 738.
- [41] S. Liu, T. Chen, X. Chen, X. Chen, Q. Xiao, B. Wu, M. Pechenizkiy, D. C. Mocanu, and Z. Wang, "More convnets in the 2020s: Scaling up kernels beyond 51x51 using sparsity," *CoRR*, vol. abs/2207.03620, 2022.
- [42] S. E. FINDER, R. Amoyal, E. Treister, and O. Freifeld, "Wavelet convolutions for large receptive fields," in *European Conference on Computer Vision*, 2024.
- [43] H. Chen, X. Chu, Y. Ren, X. Zhao, and K. Huang, "Pelk: Parameter-efficient large kernel convnets with peripheral convolution," in *Proceedings of the IEEE/CVF Conference on Computer Vision and Pattern Recognition (CVPR)*, June 2024, pp. 5557–5567.
- [44] Z. Liu, H. Mao, C.-Y. Wu, C. Feichtenhofer, T. Darrell, and S. Xie, "A convnet for the 2020s," in *Proceedings of the IEEE/CVF conference on computer vision and pattern recognition*, 2022, pp. 11 976–11 986.
- [45] Y. Zhang, X. Ding, and X. Yue, "Scaling up your kernels: Large kernel design in convnets towards universal representations," *arXiv preprint arXiv:2410.08049*, 2024.
- [46] X. Ding, X. Zhang, J. Han, and G. Ding, "Scaling up your kernels to 31x31: Revisiting large kernel design in cnns," in *Proceedings of the IEEE/CVF conference on computer vision and pattern recognition*, 2022, pp. 11 963–11 975.
- [47] F. Lin, K. Bao, Y. Li, D. Zeng, and S. Ge, "Learning contrast-enhanced shape-biased representations for infrared small target detection," *IEEE Transactions on Image Processing*, vol. 33, pp. 3047–3058, 2024.
- [48] F. Lin, S. Ge, K. Bao, C. Yan, and D. Zeng, "Learning shape-biased representations for infrared small target detection," *IEEE Transactions on Multimedia*, vol. 26, pp. 4681–4692, 2024.
- [49] M. M. Naseer, K. Ranasinghe, S. H. Khan, M. Hayat, F. Shahbaz Khan, and M.-H. Yang, "Intriguing properties of vision transformers," in *Advances in Neural Information Processing Systems*, vol. 34. Curran Associates, Inc., 2021, pp. 23 296–23 308.
- [50] K. W. Lau, L.-M. Po, and Y. A. U. Rehman, "Large separable kernel attention: Rethinking the large kernel attention design in cnn," *Expert Systems with Applications*, vol. 236, p. 121352, 2024.
- [51] G. Zhang, G. Xu, H. Wang, S. Chen, Y. Shan, and X. Zhang, "Learning dynamic local context representations for infrared small target detection," *arXiv preprint arXiv:2412.17401*, 2024.
- [52] S. Li, Z. Wang, Z. Liu, C. Tan, H. Lin, D. Wu, Z. Chen, J. Zheng, and S. Z. Li, "Moganet: Multi-order gated aggregation network," in *ICLR*, 2024.
- [53] J. Ren, D. Zhang, Y. Wang, L. Chen, Z. Zhou, Y. Chen, X. Cheng, X. Wang, M. Zhou, J. Shi *et al.*, "Towards a unified game-theoretic view of adversarial perturbations and robustness," *Advances in Neural Information Processing Systems*, vol. 34, pp. 3797–3810, 2021.
- [54] H. Deng, Q. Ren, H. Zhang, and Q. Zhang, "Discovering and explaining the representation bottleneck of dnns," 2022. [Online]. Available: <https://arxiv.org/abs/2111.06236>
- [55] Z. Chang, X. Gao, N. Li, H. Zhou, and Y. Lu, "Dnnet: Disentanglement and recombination network for few-shot semantic segmentation," *IEEE Transactions on Circuits and Systems for Video Technology*, vol. 34, no. 7, pp. 5560–5574, 2024.
- [56] H. Zhou, H. Zhang, H. Deng, D. Liu, W. Shen, S.-H. Chan, and Q. Zhang, "Explaining generalization power of a dnn using interactive concepts," ser. AAAI'24. AAAI Press, 2024.
- [57] D. Liu, H. Deng, X. Cheng, Q. Ren, K. Wang, and Q. Zhang, "Towards the difficulty for a deep neural network to learn concepts of different complexities," in *Advances in Neural Information Processing Systems*, A. Oh, T. Naumann, A. Globerson, K. Saenko, M. Hardt, and S. Levine, Eds., vol. 36. Curran Associates, Inc., 2023, pp. 41 283–41 304.
- [58] L. Tang, W. Shen, Z. Zhou, Y. Chen, and Q. Zhang, "Defects of convolutional decoder networks in frequency representation," in *Proceedings of the 40th International Conference on Machine Learning*, ser. ICML'23. JMLR.org, 2023.
- [59] M. Li and Q. Zhang, "Does a neural network really encode symbolic concepts?" in *Proceedings of the 40th International Conference on Machine Learning*, ser. ICML'23. JMLR.org, 2023.
- [60] T. Li, Z. Wen, Y. Li, and T. S. Lee, "Emergence of shape bias in convolutional neural networks through activation sparsity," *Advances in Neural Information Processing Systems*, vol. 36, pp. 71 755–71 766, 2023.
- [61] M.-H. Guo, C.-Z. Lu, Z.-N. Liu, M.-M. Cheng, and S.-M. Hu, "Visual attention network," *Computational Visual Media*, vol. 9, no. 4, pp. 733–752, 2023.
- [62] X. Dai, M. Li, P. Zhai, S. Tong, X. Gao, S.-L. Huang, Z. Zhu, C. You, and Y. Ma, "Revisiting sparse convolutional model for visual recognition," in *Advances in Neural Information Processing Systems*, vol. 35. Curran Associates, Inc., 2022, pp. 10 492–10 504.
- [63] N. H. Nazari and A. Kovashka, "The role of shape for domain generalization on sparsely-textured images," in *Proceedings of the IEEE/CVF Conference on Computer Vision and Pattern Recognition (CVPR) Workshops*, June 2022, pp. 5120–5130.
- [64] X. Zhang, X. Zhang, S.-Y. Cao, B. Yu, C. Zhang, and H.-L. Shen, "Mrf3net: An infrared small target detection network using multireceptive field perception and effective feature fusion," *IEEE Transactions on Geoscience and Remote Sensing*, vol. 62, pp. 1–14, 2024.
- [65] Y.-L. Sung, J. Cho, and M. Bansal, "Lst: Ladder side-tuning for parameter and memory efficient transfer learning," *Advances in Neural Information Processing Systems*, vol. 35, pp. 12 991–13 005, 2022.
- [66] M. Jia, L. Tang, B.-C. Chen, C. Cardie, S. Belongie, B. Hariharan, and S.-N. Lim, "Visual prompt tuning," in *European conference on computer vision*. Springer, 2022, pp. 709–727.
- [67] S. Huang, Z. Lu, K. Deb, and V. N. Boddeti, "Revisiting residual networks for adversarial robustness," in *Proceedings of the IEEE/CVF Conference on Computer Vision and Pattern Recognition*, 2023, pp. 8202–8211.
- [68] S. Hu, Z. Lou, X. Yan, and Y. Ye, "A survey on information bottleneck," *IEEE Transactions on Pattern Analysis and Machine Intelligence*, 2024.
- [69] Y. Liu, H. Li, J. Cheng, and *et al.*, "Mscaf-net: a general framework for camouflaged object detection via learning multi-scale context-aware features," *TCSVT*, 2023.
- [70] J. Zhao, X. Li, F. Yang, Q. Zhai, A. Luo, Z. Jiao, and H. Cheng, "Focusdiffuser: Perceiving local disparities for camouflaged object detection," in *European Conference on Computer Vision*. Springer, 2024, pp. 181–198.
- [71] M. Ma, C. Xia, C. Xie, X. Chen, and J. Li, "Boosting broader receptive fields for salient object detection," *IEEE Transactions on Image Processing*, 2023.
- [72] A. Radford, J. W. Kim, C. Hallacy, A. Ramesh, G. Goh, S. Agarwal, G. Sastry, A. Askell, P. Mishkin, J. Clark *et al.*, "Learning transferable visual models from natural language supervision," in *International conference on machine learning*. PmlR, 2021, pp. 8748–8763.
- [73] T. Chen, A. Lu, L. Zhu, C. Ding, C. Yu, D. Ji, Z. Li, L. Sun, P. Mao, and Y. Zang, "Sam2-adapter: Evaluating & adapting segment anything 2

- in downstream tasks: Camouflage, shadow, medical image segmentation, and more,” *arXiv preprint arXiv:2408.04579*, 2024.
- [74] W. Lin, Z. Wu, W. Yang, M. Huang, J. Huang, and L. Jin, “Hierarchical side-tuning for vision transformers,” *arXiv preprint arXiv:2310.05393*, 2023.
- [75] N. Tang, M. Fu, K. Zhu, and J. Wu, “Low-rank attention side-tuning for parameter-efficient fine-tuning,” *arXiv preprint arXiv:2402.04009*, 2024.
- [76] D. Yin, X. Han, B. Li, H. Feng, and J. Bai, “Parameter-efficient is not sufficient: Exploring parameter, memory, and time efficient adapter tuning for dense predictions,” in *Proceedings of the 32nd ACM International Conference on Multimedia*, 2024, pp. 1398–1406.
- [77] H. Zhang, C. Wu, Z. Zhang, Y. Zhu, H. Lin, Z. Zhang, Y. Sun, T. He, J. Mueller, R. Manmatha *et al.*, “Resnest: Split-attention networks,” in *Proceedings of the IEEE/CVF conference on computer vision and pattern recognition*, 2022, pp. 2736–2746.
- [78] S.-H. Gao, M.-M. Cheng, K. Zhao, X.-Y. Zhang, M.-H. Yang, and P. Torr, “Res2net: A new multi-scale backbone architecture,” *IEEE transactions on pattern analysis and machine intelligence*, vol. 43, no. 2, pp. 652–662, 2019.
- [79] Y. Chen, X. Yuan, J. Wang, R. Wu, X. Li, Q. Hou, and M.-M. Cheng, “Yolo-ms: rethinking multi-scale representation learning for real-time object detection,” *IEEE Transactions on Pattern Analysis and Machine Intelligence*, 2025.
- [80] L. Fan, Y. Wang, G. Hu, F. Li, Y. Dong, H. Zheng, C. Lin, Y. Huang, and X. Ding, “Diffusion-based continuous feature representation for infrared small-dim target detection,” *IEEE Transactions on Geoscience and Remote Sensing*, vol. 62, pp. 1–17, 2024.
- [81] G. Yue, S. Wu, T. Zhou, G. Li, J. Du, Y. Luo, and Q. Jiang, “Progressive region-to-boundary exploration network for camouflaged object detection,” *IEEE Transactions on Multimedia*, vol. 27, pp. 236–248, 2025.
- [82] M. Zhang, K. Yue, J. Zhang, Y. Li, and X. Gao, “Exploring feature compensation and cross-level correlation for infrared small target detection,” in *Proceedings of the 30th ACM International Conference on Multimedia*, ser. MM ’22. New York, NY, USA: Association for Computing Machinery, 2022, p. 1857–1865.
- [83] W. Yu, P. Zhou, S. Yan, and X. Wang, “Inceptionnext: When inception meets convnext,” in *Proceedings of the IEEE/CVF Conference on Computer Vision and Pattern Recognition*, 2024, pp. 5672–5683.
- [84] M.-H. Guo, C.-Z. Lu, Q. Hou, Z. Liu, M.-M. Cheng, and S.-M. Hu, “Segnext: Rethinking convolutional attention design for semantic segmentation,” *Advances in Neural Information Processing Systems*, vol. 35, pp. 1140–1156, 2022.
- [85] Y. Li, X. Li, Y. Dai, Q. Hou, L. Liu, Y. Liu, M.-M. Cheng, and J. Yang, “Lsknet: A foundation lightweight backbone for remote sensing,” *International Journal of Computer Vision*, pp. 1–22, 2024.
- [86] Y. Li, Q. Hou, Z. Zheng, M.-M. Cheng, J. Yang, and X. Li, “Large selective kernel network for remote sensing object detection,” in *Proceedings of the IEEE/CVF International Conference on Computer Vision*, 2023, pp. 16 794–16 805.
- [87] G. Xu, G. Zhang, L. Ye, S. Gan, X. Zhang, and X. Yang, “Optimizing local-global dependencies for accurate 3d human pose estimation,” *arXiv preprint arXiv:2412.19676*, 2024.
- [88] M. Oquab, T. Darcet, T. Moutakanni, H. Vo, M. Szafraniec, V. Khalidov, P. Fernandez, D. Haziza, F. Massa, A. El-Nouby *et al.*, “Dinov2: Learning robust visual features without supervision,” *arXiv preprint arXiv:2304.07193*, 2023.
- [89] M. I. Belghazi, A. Baratin, S. Rajeshwar, S. Ozair, Y. Bengio, A. Courville, and D. Hjelm, “Mutual information neural estimation,” in *International conference on machine learning*. PMLR, 2018, pp. 531–540.
- [90] Y. Wang, R. Wang, X. Fan, T. Wang, and X. He, “Pixels, regions, and objects: Multiple enhancement for salient object detection,” in *Proceedings of the IEEE/CVF Conference on Computer Vision and Pattern Recognition*, 2023, pp. 10 031–10 040.
- [91] F. Locatello, S. Bauer, M. Lucic, G. Raetsch, S. Gelly, B. Schölkopf, and O. Bachem, “Challenging common assumptions in the unsupervised learning of disentangled representations,” in *international conference on machine learning*. PMLR, 2019, pp. 4114–4124.
- [92] W. Yu, M. Luo, P. Zhou, C. Si, Y. Zhou, X. Wang, J. Feng, and S. Yan, “Metaformer is actually what you need for vision,” in *Proceedings of the IEEE/CVF conference on computer vision and pattern recognition*, 2022, pp. 10 819–10 829.
- [93] W. Yu, C. Si, P. Zhou, M. Luo, Y. Zhou, J. Feng, S. Yan, and X. Wang, “Metaformer baselines for vision,” *IEEE Transactions on Pattern Analysis and Machine Intelligence*, 2023.
- [94] Y. Wu and K. He, “Group normalization,” in *Proceedings of the European conference on computer vision (ECCV)*, 2018, pp. 3–19.
- [95] H. Touvron, M. Cord, A. Sablayrolles, G. Synnaeve, and H. Jégou, “Going deeper with image transformers,” in *Proceedings of the IEEE/CVF international conference on computer vision*, 2021, pp. 32–42.
- [96] I. O. Tolstikhin, N. Houlsby, A. Kolesnikov, L. Beyer, X. Zhai, T. Unterthiner, J. Yung, A. Steiner, D. Keysers, J. Uszkoreit *et al.*, “Mlp-mixer: An all-mlp architecture for vision,” *Advances in neural information processing systems*, vol. 34, pp. 24 261–24 272, 2021.
- [97] Z. Chen, Y. Duan, W. Wang, J. He, T. Lu, J. Dai, and Y. Qiao, “Vision transformer adapter for dense predictions,” *arXiv preprint arXiv:2205.08534*, 2022.
- [98] Q. Hou, C.-Z. Lu, M.-M. Cheng, and J. Feng, “Conv2former: A simple transformer-style convnet for visual recognition,” *IEEE Transactions on Pattern Analysis and Machine Intelligence*, 2024.
- [99] H. Xing, Y. Wang, X. Wei, and *et al.*, “Go closer to see better: Camouflaged object detection via object area amplification and figure-ground conversion,” *TCSVT*, 2023.
- [100] Z. Huang, H. Dai, T.-Z. Xiang, and *et al.*, “Feature shrinkage pyramid for camouflaged object detection with transformers,” in *CVPR*, 2023, pp. 5557–5566.
- [101] X. Hu, S. Wang, X. Qin, and *et al.*, “High-resolution iterative feedback network for camouflaged object detection,” in *AAAI*, vol. 37, no. 1, 2023, pp. 881–889.
- [102] Y. Yang and Q. Zhang, “Finding camouflaged objects along the camouflage mechanisms,” *IEEE Transactions on Circuits and Systems for Video Technology*, vol. 34, no. 4, pp. 2346–2360, 2024.
- [103] Z. Liu, X. Deng, P. Jiang, C. Lv, G. Min, and X. Wang, “Edge perception camouflaged object detection under frequency domain reconstruction,” *IEEE Transactions on Circuits and Systems for Video Technology*, vol. 34, no. 10, pp. 10 194–10 207, 2024.
- [104] Y. Wang, X. Bi, B. Liu, Y. Wei, W. Li, and B. Xiao, “Learning discriminative representations from cross-scale features for camouflaged object detection,” *IEEE Transactions on Circuits and Systems for Video Technology*, vol. 34, no. 12, pp. 12 756–12 769, 2024.
- [105] X. Song, P. Zhang, X. Lu, X. Hei, and R. Liu, “A universal multi-view guided network for salient object and camouflaged object detection,” *IEEE Transactions on Circuits and Systems for Video Technology*, vol. 34, no. 11, pp. 11 184–11 197, 2024.
- [106] B. Yin, X. Zhang, D.-P. Fan, S. Jiao, M.-M. Cheng, L. Van Gool, and Q. Hou, “Camoforner: Masked separable attention for camouflaged object detection,” *IEEE Transactions on Pattern Analysis and Machine Intelligence*, vol. 46, no. 12, pp. 10 362–10 374, 2024.
- [107] L. Wang, J. Yang, Y. Zhang, F. Wang, and F. Zheng, “Depth-aware concealed crop detection in dense agricultural scenes,” in *Proceedings of the IEEE/CVF Conference on Computer Vision and Pattern Recognition*, 2024, pp. 17 201–17 211.
- [108] S. Yao, H. Sun, T.-Z. Xiang, X. Wang, and X. Cao, “Hierarchical graph interaction transformer with dynamic token clustering for camouflaged object detection,” *IEEE Transactions on Image Processing*, vol. 33, pp. 5936–5948, 2024.
- [109] C. Hao, Z. Yu, X. Liu, J. Xu, H. Yue, and J. Yang, “A simple yet effective network based on vision transformer for camouflaged object and salient object detection,” *IEEE Transactions on Image Processing*, vol. 34, pp. 608–622, 2025.
- [110] V. Asnani, A. Kumar, S. You, and X. Liu, “Probed: Proactive object detection wrapper,” *Advances in Neural Information Processing Systems*, vol. 36, pp. 77 993–78 005, 2023.
- [111] J. Yang, B. Zhong, Q. Liang, Z. Mo, S. Zhang, and S. Song, “Uncertainty-guided diffusion model for camouflaged object detection,” *IEEE Transactions on Multimedia*, pp. 1–14, 2025.
- [112] K. Sun, Z. Chen, X. Lin, X. Sun, H. Liu, and R. Ji, “Conditional diffusion models for camouflaged and salient object detection,” *IEEE Transactions on Pattern Analysis and Machine Intelligence*, vol. 47, no. 4, pp. 2833–2848, 2025.
- [113] T. Chen, L. Zhu, C. Deng, and *et al.*, “Sam-adapter: Adapting segment anything in underperformed scenes,” in *ICCVW*, 2023, pp. 3367–3375.
- [114] L. Zhang, Q. Zhang, and R. Zhao, “Progressive dual-attention residual network for salient object detection,” *IEEE Transactions on Circuits and Systems for Video Technology*, vol. 32, no. 9, pp. 5902–5915, 2022.
- [115] Q. Zhang, R. Zhao, and L. Zhang, “Tnet: A trifurcated cascaded refinement network for salient object detection,” *IEEE Transactions on Circuits and Systems for Video Technology*, vol. 33, no. 1, pp. 298–311, 2023.
- [116] X. Zhou, K. Shen, and Z. Liu, “Admnet: Attention-guided densely multi-scale network for lightweight salient object detection,” *IEEE Transactions on Multimedia*, vol. 26, pp. 10 828–10 841, 2024.

- [117] J. Liu, J. Zhang, and N. Barnes, "Modeling aleatoric uncertainty for camouflaged object detection," in *WACV*, 2022, pp. 1445–1454.
- [118] Z. Fu, R. Chen, Y. Huang, E. Cheng, X. Ding, and K.-K. Ma, "Masnet: A robust deep marine animal segmentation network," *IEEE Journal of Oceanic Engineering*, 2023.
- [119] T. Chen, L. Zhu, C. Ding, R. Cao, S. Zhang, Y. Wang, Z. Li, L. Sun, P. Mao, and Y. Zang, "Sam fails to segment anything?—sam-adapter: Adapting sam in underperformed scenes: Camouflage, shadow, and more," *arXiv*, 2023.
- [120] Y. Lai, Z. Luo, and Z. Yu, "Detect any deepfakes: Segment anything meets face forgery detection and localization," *arXiv*, 2023.
- [121] P. Zhang, T. Yan, Y. Liu, and H. Lu, "Fantastic animals and where to find them: Segment any marine animal with dual sam," in *Proceedings of the IEEE/CVF Conference on Computer Vision and Pattern Recognition*, 2024, pp. 2578–2587.
- [122] W. Wu, W. Yang, W. Ma, and X.-D. Chen, "How many annotations do we need for generalizing new-coming shadow images?" *IEEE Transactions on Circuits and Systems for Video Technology*, vol. 33, no. 11, pp. 6213–6224, 2023.
- [123] X.-D. Chen, W. Wu, W. Yang, H. Qin, X. Wu, and X. Mao, "Make segment anything model perfect on shadow detection," *IEEE Transactions on Geoscience and Remote Sensing*, vol. 61, pp. 1–13, 2023.
- [124] X. Wang, S. Yao, Y. Tang, S. Yang, and Z. Liu, "Shadow-aware decomposed transformer network for shadow detection and removal," *Pattern Recognition*, vol. 156, p. 110771, 2024.
- [125] B. Li, C. Xiao, L. Wang, Y. Wang, Z. Lin, M. Li, W. An, and Y. Guo, "Dense nested attention network for infrared small target detection," *IEEE Transactions on Image Processing*, vol. 32, pp. 1745–1758, 2023.
- [126] X. Wu, D. Hong, and J. Chanussot, "Uiu-net: U-net in u-net for infrared small object detection," *IEEE Transactions on Image Processing*, vol. 32, pp. 364–376, 2023.
- [127] T. Wu, B. Li, Y. Luo, Y. Wang, C. Xiao, T. Liu, J. Yang, W. An, and Y. Guo, "Mtu-net: Multilevel transunet for space-based infrared tiny ship detection," *IEEE Transactions on Geoscience and Remote Sensing*, vol. 61, pp. 1–15, 2023.
- [128] Y. Dai, P. Pan, Y. Qian, Y. Li, X. Li, J. Yang, and H. Wang, "Pick of the bunch: Detecting infrared small targets beyond hit-miss trade-offs via selective rank-aware attention," *IEEE Transactions on Geoscience and Remote Sensing*, vol. 62, pp. 1–15, 2024.
- [129] Q. Liu, R. Liu, B. Zheng, H. Wang, and Y. Fu, "Infrared small target detection with scale and location sensitivity," in *Proceedings of the IEEE/CVF Computer Vision and Pattern Recognition*, 2024.
- [130] X. Yang, H. Mei, K. Xu, X. Wei, B. Yin, and R. W. Lau, "Where is my mirror?" in *Proceedings of the IEEE/CVF International Conference on Computer Vision*, 2019, pp. 8809–8818.
- [131] J. Lin, G. Wang, and R. W. Lau, "Progressive mirror detection," in *Proceedings of the IEEE/CVF conference on computer vision and pattern recognition*, 2020, pp. 3697–3705.
- [132] N. Liu, N. Zhang, K. Wan, L. Shao, and J. Han, "Visual saliency transformer," in *ICCV*, 2021.
- [133] H. Guan, J. Lin, and R. W. Lau, "Learning semantic associations for mirror detection," in *Proceedings of the IEEE/CVF Conference on Computer Vision and Pattern Recognition*, 2022, pp. 5941–5950.
- [134] X. Tan, J. Lin, K. Xu, P. Chen, L. Ma, and R. W. Lau, "Mirror detection with the visual chirality cue," *IEEE Transactions on Pattern Analysis and Machine Intelligence*, vol. 45, no. 3, pp. 3492–3504, 2022.
- [135] T. Huang, B. Dong, J. Lin, X. Liu, R. W. Lau, and W. Zuo, "Symmetry-aware transformer-based mirror detection," in *Proceedings of the aaai conference on artificial intelligence*, vol. 37, no. 1, 2023, pp. 935–943.
- [136] M. Zha, F. Fu, Y. Pei, G. Wang, T. Li, X. Tang, Y. Yang, and H. T. Shen, "Dual domain perception and progressive refinement for mirror detection," *IEEE Transactions on Circuits and Systems for Video Technology*, 2024.
- [137] T.-N. Le, T. V. Nguyen, Z. Nie, M.-T. Tran, and A. Sugimoto, "Anabranch network for camouflaged object segmentation," *Computer vision and image understanding*, vol. 184, pp. 45–56, 2019.
- [138] D.-P. Fan, G.-P. Ji, G. Sun, M.-M. Cheng, J. Shen, and L. Shao, "Camouflaged object detection," in *CVPR*, 2020, pp. 2777–2787.
- [139] P. Skurkowski, H. Abdulameer, J. Błaszczyk, T. Depta, A. Kornacki, and P. Koziel, "Animal camouflage analysis: Chameleon database," *Unpublished manuscript*, vol. 2, no. 6, p. 7, 2018.
- [140] Y. Lv, J. Zhang, Y. Dai, A. Li, B. Liu, N. Barnes, and D.-P. Fan, "Simultaneously localize, segment and rank the camouflaged objects," in *CVPR*, 2021, pp. 11 591–11 601.
- [141] L. Wang, H. Lu, Y. Wang, M. Feng, D. Wang, B. Yin, and X. Ruan, "Learning to detect salient objects with image-level supervision," in *Proceedings of the IEEE conference on computer vision and pattern recognition*, 2017, pp. 136–145.
- [142] C. Yang, L. Zhang, H. Lu, X. Ruan, and M.-H. Yang, "Saliency detection via graph-based manifold ranking," in *Proceedings of the IEEE conference on computer vision and pattern recognition*, 2013, pp. 3166–3173.
- [143] G. Li and Y. Yu, "Visual saliency based on multiscale deep features," in *Proceedings of the Conference on Computer Vision and Pattern Recognition (CVPR)*, 2015.
- [144] Y. Li, X. Hou, C. Koch, J. M. Rehg, and A. L. Yuille, "The secrets of salient object segmentation," in *Proceedings of the IEEE conference on computer vision and pattern recognition*, 2014, pp. 280–287.
- [145] Q. Yan, L. Xu, J. Shi, and J. Jia, "Hierarchical saliency detection," in *Proceedings of the IEEE conference on computer vision and pattern recognition*, 2013, pp. 1155–1162.
- [146] T. Zhang, L. Li, S. Cao, T. Pu, and Z. Peng, "Attention-guided pyramid context networks for detecting infrared small target under complex background," *IEEE Transactions on Aerospace and Electronic Systems*, vol. 59, no. 4, pp. 4250–4261, 2023.
- [147] J. Wang, X. Li, and J. Yang, "Stacked conditional generative adversarial networks for jointly learning shadow detection and shadow removal," in *Proceedings of the IEEE conference on computer vision and pattern recognition*, 2018, pp. 1788–1797.
- [148] D. Yin, L. Hu, B. Li, Y. Zhang, and X. Yang, "5%>100%: Breaking performance shackles of full fine-tuning on visual recognition tasks," 2024. [Online]. Available: <https://arxiv.org/abs/2408.08345>



Guoyi Zhang received the B.E. degree from Hefei University of Technology, Hefei, China, in 2023. He is currently pursuing the M.E. degree with the School of Aeronautics and Astronautics, Sun Yat-sen University, Shenzhen, China. His current research interests include representation learning and infrared small target detection.



Siyang Chen received the B.E. degree from Sun Yat-sen University, Shenzhen, China, in 2023. He is currently pursuing the M.E. degree with the School of Aeronautics and Astronautics, Sun Yat-sen University, Shenzhen, China. His research interests include space resident object detection and infrared small target detection.



Guangsheng Xu received the B.E. degree from Sun Yat-sen University, Shenzhen, China, in 2023. He is currently pursuing the M.E. degree with the School of Aeronautics and Astronautics, Sun Yat-sen University, Shenzhen, China. His current research interests include human pose estimation and human shape reconstruction.



Han Wang received the B.E. degree in mechanical engineering from Nanjing Agricultural University, Nanjing, China, in 2020, and the M.E. degree in mechanical engineering from China Agriculture University, Beijing, China, in 2022. He is currently working toward the Ph.D. degree with the School of Aeronautics and Astronautics, Sun Yat-sen University, Shenzhen, China. His research interests include astronomical image processing and space debris detection.



Xiaohu Zhang received the Ph.D. degree in aeronautical and astronautical science and technology from National University of Defense Technology, Changsha, China, in 2006. He is currently a Professor with the School of Aeronautics and Astronautics, Sun Yat-sen University, Shenzhen, China. His research interests include aircraft visual perception, computer vision, and photogrammetry.